JACS
JOURNAL OF THE AMERICAN CHEMICAL SOCIETY
Article
Cite This: J. Am. Chem. Soc. 2019, 141, 1970−1979
pubs.acs.org/JACS

Degradation of Cytosine Radical Cations in 2′-Deoxycytidine and in i-Motif DNA: Hydrogen-Bonding Guided Pathways

Yinghui Wang,[†,‡,§,∥] Hongmei Zhao,[‡,∥] Chunfan Yang,[†] Jialong Jie,[†] Xiaojuan Dai,[†] Qian Zhou,[†] Kunhui Liu,[†] Di Song,[‡] and Hongmei Su*[,†]

[†]College of Chemistry, Beijing Normal University, Beijing 100875, P. R. China
[‡]Beijing National Laboratory for Molecular Science, Institute of Chemistry, Chinese Academy of Science, Beijing 100190, P. R. China
[§]University of Chinese Academy of Science, Beijing 100049, P. R. China

Supporting Information

ABSTRACT: Radical cations of nucleobases are key intermediates causing genome mutation, among which cytosine $C^{\bullet+}$ is of growing importance because the ensuing cytosine oxidation causes GC → AT transversions in DNA replication. Although the chemistry and biology of steady-state C oxidation products have been characterized, time-resolved study of initial degradation pathways of $C^{\bullet+}$ is still at the preliminary stage. Herein, we choose i-motif, a unique C-quadruplex structure composed of hemiprotonated base pairs $C(H)^+$:C, to examine $C^{\bullet+}$ degradation in a DNA surrounding without interference of G bases. Comprehensive time-resolved spectroscopy were performed to track $C^{\bullet+}$ dynamics in i-motif and in free base dC. The competing pathways of deprotonation (1.4×10^7 s^{-1}), tautomerization (8.8×10^4 s^{-1}), and hydration (5.3×10^3 s^{-1}) are differentiated, and their rate constants are determined for the first time, underlining the strong reactivity of $C^{\bullet+}$. Distinct pathway is observed in i-motif compared with dC, showing the prominent features of $C^{\bullet+}$ hydration forming $C(5OH)^{\bullet}$ and $C(6OH)^{\bullet}$. By further experiments of pH-dependence, comparison with single strand, and with Ag^+ mediated i-motif, the mechanisms of $C^{\bullet+}$ degradation in i-motif are disclosed. The hydrogen-bonding within $C(H)^+$:C plays a significant role in guiding the reaction flux, by blocking the tautomerization of $C(-H)^{\bullet}$ and reversing the equilibrium from $C(-H)^{\bullet}$ to $C^{\bullet+}$. The C radicals in i-motif thus retain more cation character, and are mainly subject to hydration leading to lesion products that can induce disruption of i-motif structure and affect its critical roles in gene-regulation.

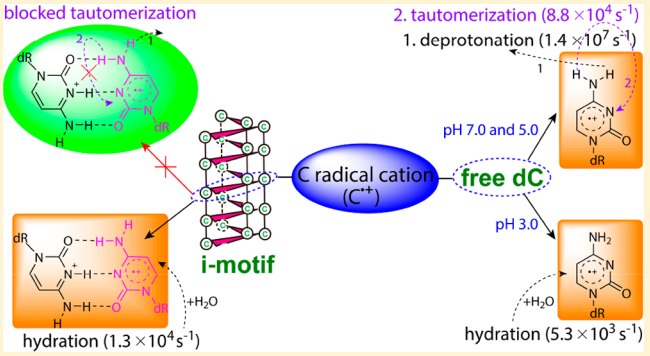

INTRODUCTION

DNA and other biomolecules of living systems may be oxidatively damaged by exposing them to endogenously generated oxygen species or by a large number of exogenous chemical and physical agents,[1] which play significant roles in the pathophysiology of inflammation, cancer, and degenerative diseases.[2,3] One of the most potent sources of exogenous DNA damage is the one-electron oxidation of nucleobases, which can occur during the exposure of DNA to ionizing radiation or photosensitizers.[4,5] Numerous efforts have been made in the last two decades on the delineation of molecular mechanisms of ionizing radiation damage on cellular DNA.[1,6−8] Evidence is now accumulating that the radical cations of DNA bases generated by the ionizing radiation initiate a variety of physical and chemical alterations, constituting one of the main types of cytotoxic DNA lesions.[7,9−12] Thus, investigations on the degradation pathways of radical cations can provide guidance for understanding the mechanisms of DNA damage caused by ionizing radiation or chemical agents.

Until now, there has been increased attention on the radical cations of DNA bases and their degradation reactions,[9,13−22] among which the radical cation of guanine ($G^{\bullet+}$) has been of great interest because of the lowest oxidation potential of guanine among the four DNA bases (G < A < C < T). Competitive pathways of hydration and deprotonation subsequent to the formation of the $G^{\bullet+}$ were revealed. According to previous studies, in acid solutions (pH 2.5) when deprotonation is inhibited, hydration of $G^{\bullet+}$ is the principal pathway, resulting in the formation of 8-oxo-7,8-dihydro-2′-deoxyguanosine (8-oxoG) lesions. The hydration reaction occurs slowly with the rate constant of 3.0×10^2 s^{-1}.[23] However, in the neutral solution, the hydration reaction of $G^{\bullet+}$ in single-strand DNA and in free 2′-deoxyguanosine (dG) are negligible,[24] due to the fact that hydration of $dG^{\bullet+}$ cannot compete with the fast deprotonation (1.8×10^7 s^{-1}).[13]

Received: October 5, 2018
Published: January 9, 2019

DOI: 10.1021/jacs.8b10743
J. Am. Chem. Soc. 2019, 141, 1970−1979

It is also noteworthy that upon ionizing irradiation, the four base radical cations are formed with similar efficiency,[25] including the radical cation of cytosine ($C^{\bullet+}$). The one-electron oxidized $C^{\bullet+}$ can initiate a cascade of reactions (Scheme 1) leading to the C oxidation products (5-OH-dC

Scheme 1. $C^{\bullet+}$ Degradation Pathways Following One-Electron Oxidation of dC, Including Transient Radicals Studied in This Work and Successive Stable Products (Within the Dashed Line Frame) In Literature

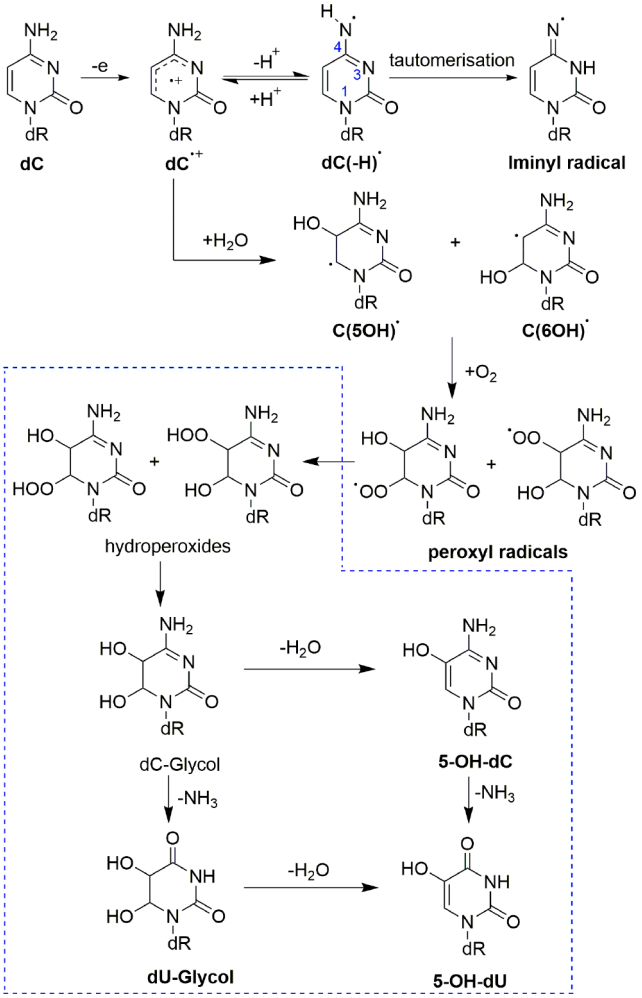

and dC-Glycol), followed by deamination to uracil derivatives 5-OH-dU and dU-Glycol.[7,26] Cytosine oxidation causes the induced deamination (i.e., C → U with a consequent change in the base pairing from G to A) and results in GC → AT transversions, which is the most common mutation type in aerobic organisms and cancer cells.[26,27] This is probably even more important than the $G^{\bullet+}$ degradation product 8-oxoG, which causes the next common mutation type G → T transversions (with ~2-fold less frequency).[26] Previous studies have focused on the chemistry and biology of the final and stable C oxidation products.[26,28−30] Although the mutagenic consequences of steady-state C oxidation products have been well characterized, time-resolved study tracking the initial degradation pathway of $C^{\bullet+}$ is still at preliminary stage.[31−34] The kinetics rate constants of the $C^{\bullet+}$ degradation in the free base dC have not even been obtained, and none of the time-resolved detection was performed on the $C^{\bullet+}$ degradation in DNA structure due to the interference of G base as hole sinks.

According to EPR and pulse radiolysis studies,[33−36] $C^{\bullet+}$ generated in 2′-deoxycytidine (dC) primarily undergoes deprotonation from the NH_2 group forming the aminyl radical $dC(-H)^{\bullet}$, which is followed by tautomerization to the iminyl radical (Scheme 1). Only a small amount of hydration products, 5-hydroxy-6-yl-2′-deoxycytidine radical $C(5OH)^{\bullet}$ and 6-hydroxy-5-yl-2′-deoxycytidine radical $C(6OH)^{\bullet}$ were indicated, based on the observation that the presence of dioxygen eliminated a fraction of spectral intensity as the OH-adduct radicals can be readily converted to their corresponding peroxyl radicals by dioxygen (Scheme 1).[7,33] Interestingly, in cellular DNA $C^{\bullet+}$ hydration seemed to become significant as manifested by the substantial increase of corresponding steady-state products 5-OH-dC, dU-Glycol and 5-OH-dU, when calf thymus DNA was exposed to γ-radiation or irradiation with near-UV light in the presence of menadione as photo-oxidant to generate DNA radical cation.[28] Substantial distribution of 5-OH-dC was also observed in the DNA of human HeLa cells upon 266 nm two-photon ionization radiation, and was thought to be originated from $C^{\bullet+}$ hydration.[7,29]

The strikingly different product yields in cellular double strand DNA from that in the free base indicates that the degradation pathways of $C^{\bullet+}$ could be highly structure-dependent. i-Motif (C quadruplex) is a unique DNA secondary structure formed by cytosine-rich sequences through a network of interdigitated hemiprotonated base pair $C(H)^+$:C at slightly acidic condition.[37] As shown in Scheme 2, the intrabase-pair

Scheme 2. Model Structures of Hemi-Protonated Base Pair $C(H)^+$:C in i-Motif and G:C Base Pair in Duplex DNA

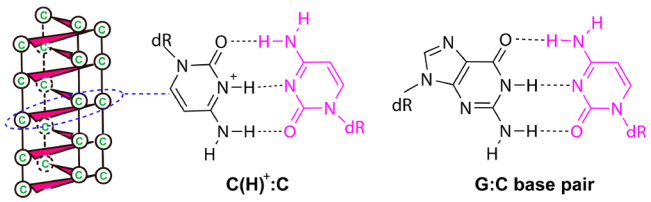

hydrogen bonding structure in i-motif DNA is quite similar to double strand DNA. We choose i-motif as a candidate to explore the decay pathways of $C^{\bullet+}$ following one-electron oxidation in a DNA surrounding without the interference of G bases, from which valuable clues to understand one-electron oxidative damage of cytosine in DNA structure could be obtained.

Importantly, i-motif DNA has been observed in the promoter region of oncogenes, making them the attractive targets for gene-regulation and anticancer therapeutics.[38−40] Far from being the transient structure, the i-motif actually mediates important regulatory roles in gene expression, acting as transcription activators.[40] Not only being observed at acidic pH below the physiological range, the i-motif structures have also been very recently discovered under physiological conditions in the nuclei of human cells.[41] Thus, research on one-electron oxidation of i-motif DNA has biological significance on its own.

Herein, by comprehensive time-resolved spectroscopy experiments, we directly monitored the degradation pathways of $C^{\bullet+}$ in free base dC and in i-motif structures. By pH-controlled measurements, the deprotonation (both deproto-

DOI: 10.1021/jacs.8b10743
J. Am. Chem. Soc. 2019, 141, 1970−1979

nation and the subsequent tautomerization) and hydration pathways of $C^{\bullet+}$ in free base dC are clearly identified and separately tracked in real time. For the first time, the elementary reaction rate constants are determined for deprotonation (1.4×10^7 s^{-1}), tautomerization (8.8×10^4 s^{-1}), and hydration (5.3×10^3 s^{-1}), respectively, providing key kinetics data for evaluating contribution of each competing pathways. Interestingly, distinct pathway is observed in i-motif DNA compared with dC at the same pH, showing the prominent features of $C^{\bullet+}$ hydration forming the $C(5OH)^{\bullet}$ and $C(6OH)^{\bullet}$. By further experiments of pH-dependence (5.0 and 6.5), comparison with the counterpart single strand, and with Ag^+ mediated i-motif, the elementary reaction mechanisms of $C^{\bullet+}$ degradation in i-motif DNA are disclosed. It shows that the intrabase pair hydrogen bonding can hinder the transformation of $C(-H)^{\bullet}$ into its more stable tautomer iminyl radical, and thus may reverse the deprotonation equilibrium from $C(-H)^{\bullet}$ to $C^{\bullet+}$. The C radical in i-motif retains more cation character, and is mainly subject to hydration. These results reveal the significant roles of the hydrogen bonding microenvironment in governing the reaction pathway of $C^{\bullet+}$, and provide an in-depth perspective to understand DNA damage associating with C oxidation. In particular for i-motif, our study demonstrates its susceptibility of C oxidative damage leading to disruption of i-motif structure and poses a new impact for this crucial noncanonical DNA secondary structure.

MATERIALS AND METHODS

Materials. 2′-Deoxycytidine (dC) and sodium persulfate were purchased from TCI and Sigma, respectively. The sodium phosphate buffers in H_2O were purchased from Beijing Solarbio Science & Technology Co., Ltd. The DNA oligonucleotides TC_3T, TC_5, and $C_3(TC_3)_3$ were purchased from Sangon Biotech (shanghai) Co., Ltd. in the HPLC/PAGE-purified form. Single-strand concentrations were determined by monitoring the absorbance at 260 nm in the UV−vis spectra and the corresponding extinction coefficients of 38 400, 45 000, and 110 900 $M^{-1}cm^{-1}$ for TC_3T, TC_5, and $C_3(TC_3)_3$ were obtained from www.idtdna.com. The i-motif DNA was prepared as follows. The oligonucleotide samples were dissolved in 50 mM sodium phosphate buffer solution and then incubated at 4 °C overnight. The formation of i-motif DNAs was confirmed by UV−vis spectroscopy and circular dichroism spectroscopy. All of the reagents were used as-received.

Laser Flash Photolysis. Nanosecond time-resolved transient absorption spectra were measured using the laser flash photolysis setup Edinburgh LP920 spectrometer (Edinburgh Instruments, Ltd.), combined with a nanosecond Nd:YAG laser (SureliteII, Continuum Inc.). The samples were excited by 355 nm laser pulse (1 Hz, 20 mJ/pulse, fwhm ≈ 7 ns). The analyzing light was from a 450 W pulsed xenon lamp. A monochromator equipped with a photomultiplier for collecting the spectral range from 300 to 700 nm was used to record transient absorption spectra. Data were analyzed by the online software of the LP920 spectrophotometer.

Circular Dichroism Spectroscopy. Circular dichroism experiments were performed at room temperature using a Jasco-815 spectropolarimeter. Each measurement was recorded from 200 to 340 nm in a 1 cm path length quartz cuvette at a scanning rate of 100 nm/min. The final data were the average of three measurements. The scan of the buffer alone was used as the background, which was subtracted from the average scan for each sample.

Generation of Sulfate Radical Anions. Sulfate radical anions, $SO_4^{\bullet-}$, were generated by the photodissociation of peroxodisulfate anions ($S_2O_8^{2-}$) by nanosecond 355 nm laser pulses. Here, the precursor of $SO_4^{\bullet-}$ is $Na_2S_2O_8$.

$$S_2O_8^{2-} + h\nu \rightarrow 2SO_4^{\bullet-}$$

The $SO_4^{\bullet-}$ has a characteristic absorption band at 440 nm, which is in good agreement with the spectra reported previously.[14] The photodissociation of $S_2O_8^{2-}$ is rapid, and $SO_4^{\bullet-}$ radicals are generated within the ~14 ns laser pulse duration. The concentration of $SO_4^{\bullet-}$ (7.2 μM) can be confirmed by measuring the absorbance at 440 nm using an extinction coefficient of 1600 $M^{-1}cm^{-1}$, which is much smaller than the concentration of dC (at least 3.0 mM) and i-motif (at least 400 μM). Due to the large excess of dC and i-motif DNA, the bimolecular reactions of $SO_4^{\bullet-}$ oxidizing dC and i-motif DNAs are considered to be pseudo first-order. It is also expected that only one C base may be oxidized by $SO_4^{\bullet-}$, yielding one electron loss center in i-motif DNAs initially.

RESULTS AND DISCUSSION

Deprotonation of $dC^{\bullet+}$. One-electron oxidation of the free base dC by $SO_4^{\bullet-}$ was first examined to obtain benchmark spectra. The transient absorption spectra for dC and $Na_2S_2O_8$ at pH 7.0 obtained after 355 nm laser excitation are shown in Figure 1a, showing a strong absorption band peaking at 415

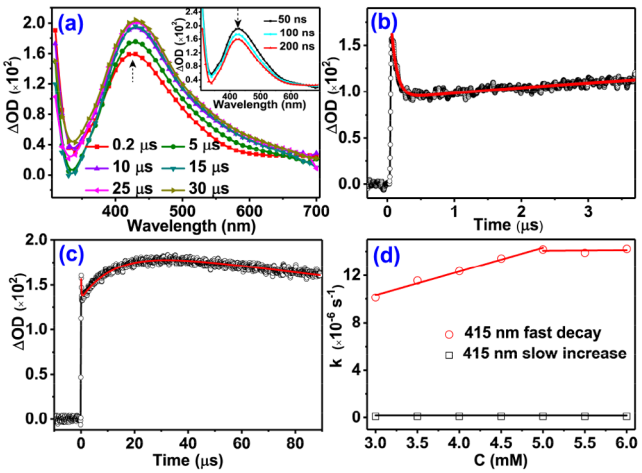

Figure 1. (a) Transient UV−vis spectra for the buffered solution (pH 7.0) of dC (6.0 mM) + $Na_2S_2O_8$ (400 mM) upon 355 nm laser flash photolysis in air; (b) shorter time scale kinetics trace to show fast decay of the 415 nm band; (c) longer time scale kinetics trace to show slow rise of the 415 nm band; solid red lines are the fitted curve; and (d) concentration dependence for the rate constants obtained from the fast decay phase (red circle) and the slow rise phase of the 415 nm band (black square) after excitation of (a) solution at pH 7.0, respectively.

nm, which should be ascribed to the one-electron oxidized product $dC^{\bullet+}$. The transient features resemble previous pulse radiolysis measurements at first glance.[32,33] But after carefully inspecting the temporal evolution of the spectra, it is found that the 415 nm band decays within the initial 0.2 μs, and as the time proceeds, the intensity increases slowly until 30 μs. These transient signals may originate from the subsequent reactions of $dC^{\bullet+}$, which should be deprotonation in the aqueous solution at neutral pH (7.0). Since the $dC^{\bullet+}$ deprotonation would be inhibited at low pH, it is thus confirmed by the pH-dependence experiments (Figure 2a−c). At pH 3.0 below the pK_a of $dC^{\bullet+}$ (4.0), the temporal behavior of the 415 nm band is obviously different due to the complete prohibition of deprotonation, showing monotonic decay. Whereas at pH 5.0, the deprotonation still occurs but becomes slower than that at pH 7.0. The pH-dependence experiments demonstrate that these signals are related to $dC^{\bullet+}$ deprotonation and its ensuing reactions.

DOI: 10.1021/jacs.8b10743
J. Am. Chem. Soc. 2019, 141, 1970−1979

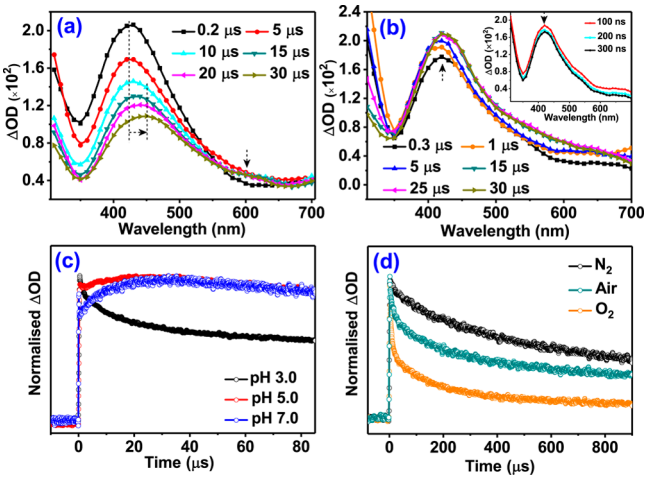

Figure 2. Transient UV−vis spectra for the buffered solution (a) at pH 3.0 (b) at pH 5.0 of dC (6.0 mM) + $Na_2S_2O_8$ (400 mM) upon 355 nm laser flash photolysis in air; (c) normalized kinetics traces of the 415 nm band at pH 3.0, 5.0 and 7.0; and (d) normalized kinetics traces of the 415 nm band in N_2, air, or O_2 -saturated conditions after excitation of (a).

At early time (before 0.2 μs), the fast decay of the 415 nm band (Figure 1a) should reflect both the oxidation of dC by $SO_4^{\bullet-}$ and $dC^{\bullet+}$ deprotonation to form $dC(-H)^{\bullet}$ since both $dC^{\bullet+}$ and $dC(-H)^{\bullet}$ have absorption at 415 nm.[33] To distinguish the oxidation of dC from $dC^{\bullet+}$ deprotonation, the kinetics traces of the fast decay at 415 nm were measured (Figure 1b) and the concentration dependence was assessed through varying the dC concentration from 3.0 to 6.0 mM. As shown in Figure 1d, the decay rate constant of 415 nm versus the concentration of dC exhibits a linear relationship below 5.0 mM, which implies that the oxidation of dC by $SO_4^{\bullet-}$ is the rate-determining step at the low dC concentration. From the slope, the second-order rate constant of dC with $SO_4^{\bullet-}$ is deduced to be 2.0×10^9 M^{-1} s^{-1}. This value is in accordance with 1.7×10^9 M^{-1} s^{-1} obtained by pulse radiolysis experiment.[33] When dC is above 5.0 mM, the rate is concentration independent, indicating that the first-order $dC^{\bullet+}$ deprotonation becomes the rate-determining step. So the plateau value of $(1.4 \pm 0.1) \times 10^7$ s^{-1} corresponds to the $dC^{\bullet+}$ deprotonation rate constant, which is as fast as that for $G^{\bullet+}$ deprotonation (1.8×10^7 s^{-1}).[13] This is reasonable considering the similar pK_a of $dC^{\bullet+}$ (4.0) to that of $dG^{\bullet+}$ (3.9).

After the fast deprotonation, the formed aminyl radical $dC(-H)^{\bullet}$ should undergo tautomerization to iminyl radical by an intramolecular hydrogen transfer from the exocyclic N4−H to N3 (Scheme 1) since the iminyl radical is 9.01 kcal/mol more stable than the aminyl radical.[34−36] So the slow rise phase at 415 nm may originate from the tautomerization from the aminyl radical to the iminyl radical. This assignment can be confirmed by the concentration dependence measurement. As shown in Figure 1d, the rate constants of the 415 nm slow rise phase are independent of the dC concentration, showing the feature of a first-order reaction. This result indicates further that the slow rise of the 415 nm band corresponds to the tautomerization of $dC(-H)^{\bullet}$, which is a first-order reaction and its rate constant is thus obtained to be $(8.8 \pm 0.2) \times 10^4$ s^{-1}. Our observations here agree with the previous time-resolved Fourier-transform EPR investigation,[34,35] in which after one-electron oxidation of 1-methylcytosine, the major product observed in nanosecond time scale was the aminyl radical $C(-H)^{\bullet}$ featured by a nitrogen (a(N4) = 1.053) and a proton (a(N4−H) = 1.744) couplings, and after 2 μs the major species was assigned to the long-lived iminyl radical with hyperfine coupling constants (hfcs) of a(N3) = 1.18, and a(N4) = 1.16. The approximate tautomerization time of 2 μs estimated from EPR agrees in general with the rate constant ($(8.8 \pm 0.2) \times 10^4$ s^{-1}) determined here by the laser flash photolysis spectroscopy. The magnitude of the rate constant also consist with the relatively high barrier of 18 kcal/mol calculated for the tautomerization at the B3LYP-PCM/6-31++G(d, p) level of theory.[42]

Hydration of $dC^{\bullet+}$. In aqueous solution of pH 7.0, $dC^{\bullet+}$ undergoes mainly deprotonation, whereas hydration could not compete with the fast deprotonation. To observe the hydration, the laser flash photolysis experiment of dC and $Na_2S_2O_8$ was performed at pH 3.0, which is lower than the pK_a (4.0) of $dC^{\bullet+}$. Under this condition, $dC^{\bullet+}$ deprotonation would be prohibited and $dC^{\bullet+}$ hydration becomes predominant. As shown in the transient spectra collected at pH 3.0 (Figure 2a), the temporal behavior of the 415 nm band is totally different. There is no fast decay followed by slow rise, the feature associated with the deprotonation of $dC^{\bullet+}$ and subsequent tautomerization. Instead, the 415 nm band intensity decays monotonically with time (Figure 2c), which is accompanied by a red shift to 440 nm as well as a weak band formation around 600 nm (Figure 2a). Presumably, these features are not related to the protonation of C base at pH 3.0. The protonation occurs with N3 of the C base, which has a pK_a of 4.3.[13] For the protonated C base $C(H)^+$ after being oxidized and losing one electron, the generated cation radical becomes acidic and the pK_a of N3 should be lowered significantly, resulting in instantaneous loss of the bound N3−H, forming $C^{\bullet+}$ again. So the 415 nm band due to $C^{\bullet+}$ was observed initially at 0.2 μs. This is the case for other bases too, e.g., one-electron oxidation of G gave rise to $G^{\bullet+}$ even in acidic pH 2.5 solution.[23] The decay of $C^{\bullet+}$ at 415 nm is concomitant with the red-shifting to 440 nm and the 600 nm build up, indicating that it should be ascribed to product formation from the subsequent reaction of $C^{\bullet+}$, which should be hydration under this acidic condition.

The hydration of $C^{\bullet+}$ is due to the nucleophilic attack of water to the C5═C6 double bond of cytosine and could result in two OH-adduct radicals, the $C(5OH)^{\bullet}$ and $C(6OH)^{\bullet}$ (Scheme 1). Are the 440 and 600 nm bands ascribed to the hydration product, the OH-adduct radicals? To aid with the assignment, the quantum chemical calculations were performed at the level of TD-B3LYP/6-311++G(d,p) with PCM to simulate bulk solvation effects. The calculated maximum absorption wavelength of $C(5OH)^{\bullet}$ and $C(6OH)^{\bullet}$ are 420 and 593 nm, respectively (Figure S1 of the Supporting Information, SI), and the calculated oscillator strength of the former radical is larger than the latter. The calculated spectral position and intensity coincide with the experiment, suggesting that the bands at 440 and 600 nm are assigned to $C(5OH)^{\bullet}$ and $C(6OH)^{\bullet}$, respectively. Moreover, the sum of the calculated spectra of $C(5OH)^{\bullet}$ and $C(6OH)^{\bullet}$ (1:1 ratio) (Figure S1) are almost identical to the 30 μs spectrum obtained in the experiment. This confirms the assignment and suggests further that the two OH-adduct radicals are formed with ~1:1 yield, which is in agreement with previous $^{18}O_2$ labeled experiment that the addition of water occurs with similar efficiency at C5 and C6 position of $dC^{\bullet+}$.[43]

DOI: 10.1021/jacs.8b10743
J. Am. Chem. Soc. 2019, 141, 1970−1979

Not only are the spectra of the two OH-adduct radicals clearly identified, but also the hydration rate constant of $dC^{\bullet+}$ can be determined. The 415 nm band consists of both the transient signals of $dC^{\bullet+}$ and OH-adduct radicals (Figure S1). To discern each of them, the kinetics traces were monitored in N_2, O_2, and air-saturated conditions (Figure 2d). It is known that OH-adduct radicals can be quenched rapidly by O_2 to generate peroxyl radicals, whereas $dC^{\bullet+}$ reacts very slowly with O_2 or not at all.[33] In N_2-saturated solution, the kinetics trace can be fitted nicely by a triexponential decay function, which contains three lifetime decay components of 15.47 μs, 183.51 μs, and a very long decay component of >1 ms, as shown in Table 1. The >1 ms component corresponds to the residual absorption lasting out of the current time window, and thus not listed in Table 1. In the O_2-saturated or the air-saturated solutions, the decay of the short lifetime component of 15.47 μs is accelerated, and the fitted time constant of this component becomes 12.12 μs (in air) and 7.77 μs (in O_2), respectively. In contrast, the other decay component of 183.51 μs is shown to be insensitive to the O_2 concentration, and the fitted time constants are 187.48 μs (in air) and 192.54 μs (in O_2). These data indicate clearly that the sharply decreased time constants following increased O_2 concentration should correspond to the OH-adduct radicals, and the decay time constant of 7.77 μs (in O_2) is in general agreement with the previously reported rate constant between OH-adduct radicals and O_2 (1.3×10^9 M^{-1} s^{-1}).[33] However, the decay component remaining unchanged in general and independent of O_2 concentration (183.51 μs, 192.54 μs, and 187.48 μs) are ascribed to the hydration of $dC^{\bullet+}$. The average of the three values then gives the hydration rate constant of $(5.3 \pm 0.1) \times 10^3$ s^{-1}.

Table 1. Decay Lifetimes Obtained from the 415 nm Band for dC and 385 nm Band for i-Motif TC_5 or i-Motif TC_3T in N_2, Air, or O_2-Saturated Conditions, Respectively[a]

	dC		i-motif TC_5		i-motif TC_3T	
	τ_1	τ_2	τ_1	τ_2	τ_1	τ_2
N_2	15.47	183.51	23.97	76.73	15.41	85.66
air	12.12	187.48	18.35	85.80	13.53	91.99
O_2	7.77	192.54	6.27	78.15	3.62	81.79

[a]The unit of these time constants is μs.

Our measurements provide knowledge of the kinetics rate constants, which is the key to evaluate contributions of respective pathways to the overall $dC^{\bullet+}$ degradation (Scheme 1). In spite of the fast deprotonation of $dC^{\bullet+}$ ($(1.4 \pm 0.1) \times 10^7$ s^{-1}), the subsequent $dC(-H)^{\bullet}$ tautomerization to form iminyl radical is slow ($(8.8 \pm 0.2) \times 10^4$ s^{-1}). So there exists an equilibrium of deprotonation and tautomerization, where the $dC^{\bullet+}$, $dC(-H)^{\bullet}$ and iminyl radical are coexisting and the equilibrium is biased to the more stable iminyl radical resulting in a small number of $dC^{\bullet+}$. Also, as the hydration is not fast ($(5.3 \pm 0.1) \times 10^3$ s^{-1}), the hydration of $dC^{\bullet+}$ thus is usually much less competitive than the deprotonation, unless when the deprotonation is prohibited at pH below the pK_a of $dC^{\bullet+}$ (4.0). For example, in the case of pulse radiolysis experiment at weak acidic conditions (pH 5.6),[33] the major part of the spectra were ascribed to deprotonated radical (N-centered) product and only a fraction was due to hydration product C-centered radicals, as was inferred from the oxygen quenching experiments.

Degradation of $C^{\bullet+}$ in i-Motif DNA. The stabilization of i-motif DNA requires slightly acidic conditions, so the laser flash photolysis experiments for i-motif DNA were performed at pH 5.0, a usual condition to ensure the i-motif formation.[37] To assist in understanding the degradation pathway of $C^{\bullet+}$ in i-motif DNA, the one-electron oxidation of the free base dC by $SO_4^{\bullet-}$ at pH 5.0 was first examined as a benchmark. As shown in Figure 2b, the spectra display fast decay at initial 0.3 μs followed by slow rise until 30 μs, which is a typical feature of the $dC^{\bullet+}$ deprotonation and the $dC(-H)^{\bullet}$ tautomerization to iminyl radical similar to the case at pH 7.0 (Figure 1a). This suggests that at pH 5.0 $dC^{\bullet+}$ still mainly undergoes deprotonation instead of hydration, in agreement with the results of the pulse radiolysis.[33] For the free base, the main degradation pathway of $dC^{\bullet+}$ is deprotonation as long as the pH is above the pK_a (4.0).

To examine the $C^{\bullet+}$degradation pathway in i-motif, we choose the cytosine-rich sequences of TC_5, which can form i-motif in 50 mM sodium phosphate buffers at pH 5.0. It is the first characterized DNA i-motif, forming an intercalated tetraplex structure under acidic conditions.[37] It consists of two parallel-stranded duplexes intercalated in an antiparallel orientation and held together by hemiprotonated $C(H)^+$:C base pairs, as shown in Figure 3a. The UV−vis absorption spectra (Figure S2) show a red shift of the maximum wavelength to 272 nm (for protonated C) from 262 nm (for neutral C), and the circular dichroism (CD) spectra (Figure S2) display a characteristic positive band around 290 nm and a negative band at 263 nm. The UV−vis and CD spectra confirm the formation of the targeted i-motif structure. Not only does it have a well-characterized structure, the i-motif TC_5 has the ascertained reaction site on the C base because the T base has higher oxidation potential and will not compete.

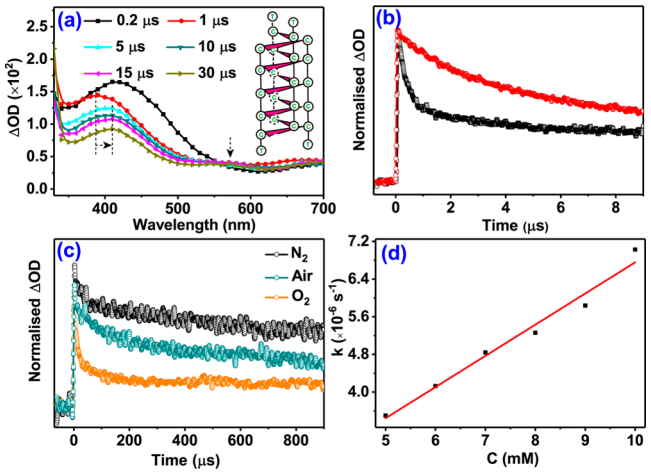

Figure 3. (a) Transient UV−vis spectra for the buffered solution at pH 5.0 of i-motif TC_5 (0.3 mM, the equivalent C concentration is 6.0 mM) + $Na_2S_2O_8$ (400 mM) upon 355 nm laser flash photolysis in air; (b) normalized kinetics traces at 440 nm after excitation of $Na_2S_2O_8$ (400 mM) solution in the absence (red circle) or presence (black square) of i-motif TC_5 ([C] = 6.0 mM); (c) normalized kinetics traces of the 385 nm band in N_2, air, or O_2-saturated conditions; and (d) concentration dependence for the rate constant obtained from the fast decay phase of 440 nm band after excitation of (a) solution at pH 5.0; red solid line is the fitting curve.

Figure 3a shows the transient absorption spectra after 355 nm laser photolysis of the mixed solution of i-motif TC_5 and

DOI: 10.1021/jacs.8b10743
J. Am. Chem. Soc. 2019, 141, 1970−1979

$Na_2S_2O_8$ at pH 5.0. The spectra essentially differ from those for the free base dC at pH 5.0 (Figure 2b), but are similar to the case of dC at pH 3.0 (Figure 2a), showing the feature of $C^{\bullet+}$ hydration. However, there are still some differences. In the transient spectra of i-motif TC_5 (Figure 3a), a new peak at 440 nm is exhibited at the initial time (0.2 μs), and as the reaction proceeds, the absorbance at 440 nm decays and shifts to 385 nm (1 μs). The 385 nm band then successively decays and shifts to 415 nm, with concomitant formation of a weak band at 550 nm within 30 μs.

The new peak at 440 nm in the 0.2 μs spectrum most probably arises from $SO_4^{\bullet-}$, since $SO_4^{\bullet-}$ have characteristic absorption centered at 440 nm.[14] Unlike free dC, the detection of the $SO_4^{\bullet-}$ band in the reaction with i-motif suggests a slower one-electron oxidation rate. Subsequent to the decay of $SO_4^{\bullet-}$ at 440 nm, the emerging bands at 385 nm, 415, and 550 nm display a temporal evolution feature similar to $dC^{\bullet+}$ hydration, indicating that the three bands may be ascribed to the $C^{\bullet+}$, $C(5OH)^{\bullet}$, and $C(6OH)^{\bullet}$, respectively. The spectral positions for these radicals in i-motif exhibit an overall blue shift compared with those in free dC, which may be related to the base stacking effect in i-motif. The influence of base stacking on spectral shift has also been observed in the $G^{\bullet+}$ deprotonation of duplex DNA.[15]

The oxidation rate of i-motif TC_5 by $SO_4^{\bullet-}$ can be obtained by following the fast decay of the 440 nm band. Figure 3b shows the $SO_4^{\bullet-}$ decay at 440 nm in the presence and absence of i-motif TC_5. Due to reacting with i-motif TC_5, the 440 nm decay of $SO_4^{\bullet-}$ is markedly accelerated compared to the slow self-decay. The concentration dependence of the kinetics at 440 nm is assessed through changing i-motif TC_5 concentration (the equivalent [C] = 5.0−10.0 mM). As shown in Figure 3d, the 440 nm fast decay rate increases as the i-motif concentration increases with linear dependence, which further indicates that the fast decay component at 440 nm is due to the bimolecular reaction of $SO_4^{\bullet-}$ with i-motif TC_5. From the slope, the second-order rate constant for the oxidation of TC_5 by $SO_4^{\bullet-}$ is deduced to be $(7.0 \pm 0.3) \times 10^8$ M^{-1} s^{-1}. The slower rate constant explains why the $SO_4^{\bullet-}$ band at 440 nm (0.2 μs) can be observed for i-motif TC_5, but not for the free base dC (2.0×10^9 M^{-1} s^{-1}). This oxidation rate constant for i-motif is comparable to that for G-quadruplex (2.1×10^9 M^{-1} s^{-1}),[14] which means that the cytosine quadruplex i-motif is also susceptible to one-electron oxidation damage.

Meanwhile, the hydration rate constant of $dC^{\bullet+}$ in i-motif can be determined by monitoring the kinetics traces of the 385 nm band in N_2, air and O_2-saturated conditions (Figure 3c), as in the case for free base dC. The time constants obtained from triexponential decay fitting are summarized in Table 1. The component independent of O_2 concentration (76.73 μs, 85.80 μs, and 78.15 μs) is ascribed to the $C^{\bullet+}$ hydration, while the component accelerated by O_2 (23.97 μs, 18.35 μs, 6.27 μs) is due to the decay of the OH-adduct radicals. Thus, the hydration rate constant of $C^{\bullet+}$ in i-motif is obtained to be $(1.3 \pm 0.2) \times 10^4$ s^{-1}, which is faster (~2 orders of magnitude) than that of $G^{\bullet+}$ (3.0×10^2 s^{-1}), and is also faster than $C^{\bullet+}$ in dC $(5.3 \pm 0.1) \times 10^3$ s^{-1}.

For $C^{\bullet+}$ and $G^{\bullet+}$, the hydration reaction is the nucleophilic addition of water to the C5═C6 double bond of $C^{\bullet+}$ or to the C8 atom of $G^{\bullet+}$.[7] The hydration reactivity should be related to the electrophile property of the radical cations. The positive charge of $G^{\bullet+}$ is distributed over both the six-membered pyrimidine ring and the five-membered imidazole ring, while in $C^{\bullet+}$ the positive charge is more concentrated since there is only one six-membered pyrimidine ring. Therefore, $C^{\bullet+}$ should be more electrophile than $G^{\bullet+}$, which makes the hydration rate of $C^{\bullet+}$ (5.3×10^3 s^{-1}) much faster than that of $G^{\bullet+}$ (3.0×10^2 s^{-1}). In i-motif due to the base pairing of C with $C(H)^+$, the $C^{\bullet+}$ after one-electron oxidation should have more cationic character, and thus becomes more electrophile than in free base dC. This should be the reason why $C^{\bullet+}$ hydration in i-motif is faster than in dC (~2-fold).

Another C-rich sequence TC_3T i-motif was also tested. The transient absorption spectra (Figure S3) obtained from the reaction of i-motif TC_3T + $SO_4^{\bullet-}$ display similar feature to that of i-motif TC_5 + $SO_4^{\bullet-}$, indicating that $C^{\bullet+}$ in i-motif TC_3T also undergo hydration to form the OH-adduct radicals. The obtained hydration rate constant is $(1.0 \pm 0.2) \times 10^4$ s^{-1} (see Table 1) and the bimolecular oxidation rate constant is $(6.6 \pm 0.2) \times 10^8$ M^{-1} s^{-1} (Figure S3).

Degradation Mechanisms of $C^{\bullet+}$ in dC and i-Motif DNA. According to the pK_a of $C^{\bullet+}$ (4.0), the $C^{\bullet+}$ in i-motif DNA at pH 5.0 should decay mainly by deprotonation. But the above experiments demonstrate clearly that the degradation of $C^{\bullet+}$ in i-motif DNA is dominated by hydration. This is quite different from the situation with the free base dC at the same pH 5.0, where the deprotonation is the major pathway. So the distinct degradation pathway of $C^{\bullet+}$ in i-motif DNA should not be caused by the slightly acidic condition. To further exclude the possibility of pH effect, we measured the $C^{\bullet+}$ degradation in $C_3(TC_3)_3$ which can form i-motif by intramolecular folding and show unexpected stability at pH 6.5 as at pH 5.0 (Figure S2).[44] Even at nearly neutral conditions, the transient absorption spectra (see Figure 4a, b) show the featured band shift from 385 to 415 nm representing hydration process (observed both at pH 5.0 and 6.5.) These observations for the three i-motif structures above point to a common fact that the deprotonation of $C^{\bullet+}$ seems to be prohibited significantly in i-motif, whereas hydration becomes the dominant pathway.

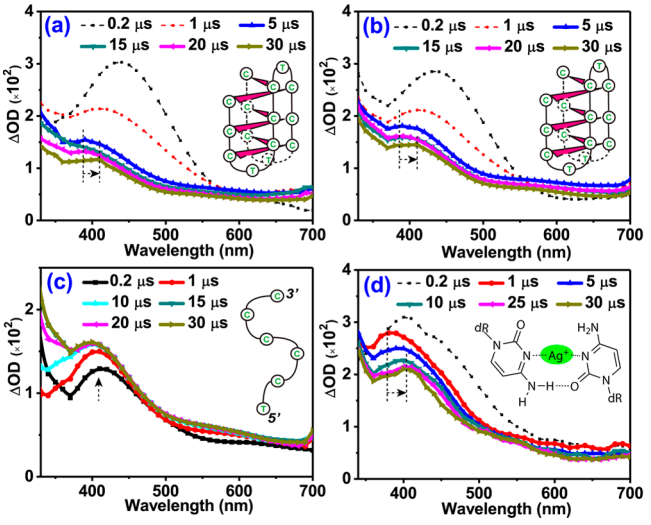

Figure 4. Transient UV−vis spectra for (a) the buffered pH 5.0 solution of $C_3(TC_3)_3$ ([C] = 6.0 mM) + $Na_2S_2O_8$ (400 mM); (b) the buffered pH 6.5 solution of $C_3(TC_3)_3$ ([C] = 6.0 mM) + $Na_2S_2O_8$ (400 mM); (c) the buffered pH 7.0 solution of ss-TC_5 ([C] = 6.0 mM) + $Na_2S_2O_8$ (400 mM); and (d) the buffered pH 7.0 solution of Ag^+ mediated i-motif $C_3(TC_3)_3$ ([C] = 6.0 mM) + $Na_2S_2O_8$ (400 mM) upon 355 nm laser flash photolysis in air.

DOI: 10.1021/jacs.8b10743
J. Am. Chem. Soc. 2019, 141, 1970−1979

Meanwhile, for the same sequence if i-motif structure cannot be formed, e.g., for TC_5 at pH 7.0 which exists only as single strand (ss-TC_5) form, the transient spectra (Figure 4c) show the feature of the deprotonated radical C(−H)• and its tautomerization. There is a slow rise of the 415 nm band until 30 μs, which resembles the case for the free base dC at pH 7.0. The comparison with its counterpart ss-TC_5 suggests that the distinct degradation pathway in i-motif should be associated with the special hydrogen bonding structure of the i-motif DNA.

Inspecting the i-motif structure, each C base is hydrogen-bonded with another protonated C base forming the $C(H)^+$:C hemiprotonated base pair as the building block. Under the attack of the highly oxidizing radical $SO_4^{\bullet-}$, which base is preferentially oxidized? In principal, the protonation should raise the oxidation potential, so the $C(H)^+$ base cannot compete with the C base when these two bases coexist. We performed PCM/B3LYP/6-31++G(d,p) level of DFT calculations, which shows clearly that the highest occupied molecular orbital (HOMO) of the $C(H)^+$:C pair is solely localized on C base but not on $C(H)^+$ (Scheme 3). The

Scheme 3. Proposed Degradation Mechanisms of $C^{\bullet+}$ in i-Motif DNA, and the Calculated Highest Occupied Molecular Orbital (HOMO) of the $C(H)^+$:C Pair at the PCM/B3LYP/6-31++G(d,p) Level

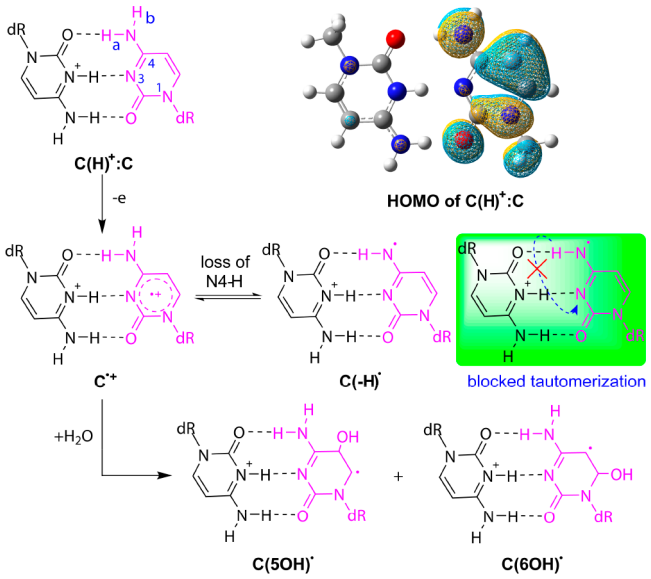

calculation results verify that the C base in i-motif DNA is the preferred electron donating site rather than $C(H)^+$. Therefore, the hole generated in i-motif DNA after one-electron oxidation is trapped in C base (highlighted in pink in Scheme 3), where the hole ($C^{\bullet+}$) may suffer from subsequent degradation by deprotonation or hydration.

According to studies with the free base dC, the $C^{\bullet+}$ deprotonation from exocyclic amino group (N4−H) to form the C(−H)• is followed by tautomerization to the iminyl radical, by the transfer of the remaining hydrogen atom from N4 to N3 (Scheme 1). The tautomeric process was calculated to be exothermic by 9.01 kcal/mol in dC.[36] The thermodynamically favorable tautomerization can then facilitate the occurrence of deprotonation, because the transformation of C(−H)• to its more stable tautomer iminyl radical simply helps to break the chemical equilibrium between $C^{\bullet+}$ and C(−H)•. Without tautomerization, the deprotonation of $C^{\bullet+}$ to C(−H)• is not complete because of the equilibrium. The involvement of tautomerization is an unusual feature for the deprotonation of cytosine cation radical.

In i-motif surroundings (Scheme 3), the N4−H_a of $C^{\bullet+}$ (pK_a 4.0) is hydrogen bonded with O2 of $C(H)^+$ with pK_a of <2.0, and proton transfer along the hydrogen bond and then release to solution is thermodynamically infeasible. Thus, the deprotonation of $C^{\bullet+}$ in i-motif DNA can only occur with the free proton N4−H_b. Subsequently, the remaining N4−H_a in the metastable product C(−H)• should migrate to N3 to form the more stable tautomer. But N4−H_a and N3 are both hydrogen bonded in the $C(H)^+$:C base pair, with O2 and $N3H^+$ of another C base, respectively. Being highly restricted by such intrabase pair hydrogen bonding, the tautomerization of C(−H)• into iminyl radical should be inhibited. Without tautomerization being followed, the chemical equilibrium of the deprotonation tends to shift in reverse to the $C^{\bullet+}$. This may be the main reason for the lack of deprotonation in i-motif DNA after one-electron oxidation. Meanwhile, since the hydration rate of $C^{\bullet+}$ in i-motif (1.2×10^4 s^{-1}) is relatively fast (2 orders of magnitude faster than that of $G^{\bullet+}$), hydration becomes the dominant degradation pathway of $C^{\bullet+}$ in i-motif.

This conclusion can be further verified by a control experiment performed for the Ag^+ mediated i-motif DNA at neutral pH. In the presence of Ag^+, the $C_3(TC_3)_3$ sequence can form i-motif structure at pH 7.0, as featured by the CD spectra (Figure S4). Its structure is formed by Ag^+ mediation, serving as H^+ to enhance the base pairing as shown in Figure 4d.[45] According to IR-MPD spectroscopy and theoretical calculations,[46] the nonconventional metal mediated base pair C−Ag^+−C mimics the structure of the hemiprotonated $C(H)^+$:C of the i-motif structure, with the formal replacement of one NH···N intermolecular bond by a stronger N···Ag^+···N bond. The high stability of this structure is suggested to be due to a synergetic effect between the strong interaction N···Ag^+ and intermolecular H-bond. This structure is asymmetric with respect to the intermolecular O(2)···N(4′) (3.3 Å) and O(2′)···N(4) (5.3 Å) distances, since Ag^+ is larger than H^+ in size and Ag^+ behaves as a soft acid. In this case, although the N4−H in C base are non-hydrogen bonded and free, the N3 site of C base are still occupied by bonding with Ag^+, the tautomerization of the deprotonated radical C(-H)• could still be prohibited and thus the deprotonation could still be prevented. Indeed, the transient absorption spectra obtained for the Ag^+ mediated i-motif are similar to i-motif TC_5 (see Figure 4d), suggesting that the predominant process is the hydration reaction instead of deprotonation. The control experiment further demonstrates that the inhibition of C(−H)• tautomerization simply prevents the occurrence of deprotonation, and the inhibition should be mainly caused by the hydrogen bonding of the N3 site of C base.

The observations of the degradation pathways of $C^{\bullet+}$ in i-motif that are notably distinct from in dC lead to insightful implications as follows:

(1) The importance of cytosine oxidation in biology can be underlined further, based on the kinetics data and mechanisms addressed here. The elementary reaction rate constants for the one-electron oxidation of C and $C^{\bullet+}$ deprotonation are both comparable to those for G, and the rate constant of $C^{\bullet+}$ hydration is ∼2 orders of magnitude faster than that of $G^{\bullet+}$ hydration. The strong

DOI: 10.1021/jacs.8b10743
J. Am. Chem. Soc. 2019, 141, 1970−1979

reactivity revealed here for $C^{\bullet+}$ can rationalize the observations that ionizing radiation of calf thymus DNA or DNA of human HeLa cells could still incur substantial amount of cytosine oxidation lesions (5-OH-C, U-Glycol, and 5-OH-U),[28,29] although the hole in C should migrate preferentially to G leading to the predominant 8-oxoG lesion. Hole transfer depends on various factors (sequence, distance, and so forth) and is not always efficient, with the rate of 10^4−10^{10} s^{-1}.[47,48] Considering the fast reaction rate constants measured here, the $C^{\bullet+}$ degradation pathways should be able to compete in some circumstances. According to the Curtin-Hammett principle, it is not the most stable (i.e., lowest E_{ox}) species in the equilibrated distribution of the radical cation that gives the major product but the one with the highest reactivity.[49] In this sense, since the rate of hydration for $C^{\bullet+}$ is much greater than $G^{\bullet+}$, it is this feature that may affect the outcome of reactions related to the hydration of radical cations. This is probably one reason why the level of C oxidation products are comparable to G in mammals.[27]

(2) The microenvironment of the hydrogen bonding structure in DNA plays significant roles in governing the reaction process. In particular for cytosine, the dominant deprotonation pathway in free base and in single stranded DNA is replaced by hydration, because hydrogen bonding in the $C(H)^+$:C base pair hinders the tautomerization of $C(-H)^{\bullet}$ into iminyl radical and thus reverses the deprotonation equilibrium from $C(-H)^{\bullet}$ to $C^{\bullet+}$. The C radical in i-motif thus retains more cation character, and is mainly subject to hydration forming $C(5OH)^{\bullet}$ and $C(6OH)^{\bullet}$.

(3) The major $C^{\bullet+}$ hydration pathway and the ensuing $C(5OH)^{\bullet}$ and $C(6OH)^{\bullet}$ formation is expected to yield deleterious consequences for the i-motif structure and stability. According to previous studies, the $C(5OH)^{\bullet}$ and $C(6OH)^{\bullet}$ are critical precursors of final lesion products.[7,30] They react with O_2 to peroxyl radicals, which then lead to the successive formation of 5-OH-dC and dC-Glycol (Scheme 1). These two oxidation products involve saturation of the 5,6-double bond of cytosine, rendering the exocyclic amino group susceptible to deamination forming 5-OH-dU and dU-Glycol.[7,30] The whole reaction initiated by $C^{\bullet+}$ hydration thus leads to C-to-U lesion. The two uracil derivatives 5-OH-dU and dU-Glycol with the removal of the NH_2 group, if formed in i-motif DNA, would incur the disappearance of NH···O bond and thus significantly weaken or destroy the hydrogen bonding within the $C(H)^+$:C base pair (Scheme 3), leading eventually to the disruption of the i-motif structure. Even a single C substitution by U caused the loss of one $C(H)^+$:C pair and thus an extensive destabilization of the i-motif structure.[50] Therefore, it is conceivable that the C-to-U lesion initiated from the $C^{\bullet+}$ hydration, can alter i-motif stability and conformation and thus affect their critical roles in gene-regulation and anticancer therapeutics that are structure-dependent. Our results disclosed for $C^{\bullet+}$ degradation pathway in i-motif thereby pose a new impact for this crucial noncanonical DNA secondary structure and provide a core foundation for future studies addressing the biological and medicinal consequences of cytosine oxidation in i-motif.

CONCLUSIONS

In summary, we have performed systematic time-resolved spectroscopy experiments and clarified the elementary degradation pathways of the cytosine radical cation $C^{\bullet+}$ in free base dC and in i-motif DNA. By carefully inspecting the different spectral pattern and temporal evolution at typical pH, the competing pathways of deprotonation, tautomerization, and hydration in free base dC are discerned from each other. For the first time, the elementary reaction rate constants are explicitly determined for deprotonation (1.4×10^7 s^{-1}), tautomerization (8.8×10^4 s^{-1}), and hydration (5.3×10^3 s^{-1}), respectively, providing key kinetics data for evaluating contribution of each competing pathways.

Intriguingly, prominent features of $C^{\bullet+}$ hydration forming the $C(5OH)^{\bullet}$ and $C(6OH)^{\bullet}$ are observed for the degradation pathway of $C^{\bullet+}$ in the i-motif formed by the C-rich sequences of TC5 or TC_3T at pH 5.0, or $C_3(TC_3)_3$ at pH 6.5, with faster hydration rate constant of $\sim 1.3 \times 10^4$ s^{-1}. This is distinct from the phenomena observed for its counterpart single strand and for free base dC at the same slightly acidic pH, where deprotonation is the principal pathway. The observations for the three i-motif structures point to a common fact that the deprotonation of $C^{\bullet+}$ is prohibited significantly in i-motif, whereas hydration becomes dominant.

Mechanistically, the markedly different pathways in i-motif should be related to the hydrogen bonding structure of the i-motif building block $C(H)^+$:C. Being highly restricted by such intrabase pair hydrogen bonding, the tautomerization of $C(-H)^{\bullet}$ into the more stable iminyl radical is easily blocked. Without tautomerization being followed, the deprotonation equilibrium tends to be reversed from $C(-H)^{\bullet}$ to $C^{\bullet+}$, rendering more cation character for the C radical. $C^{\bullet+}$ hydration ($\sim 1.3 \times 10^4$ s^{-1}) becomes the dominant degradation pathway in i-motif. These results clearly illustrate the significant roles of the hydrogen bonding structure of DNA in governing the reaction flux of $C^{\bullet+}$ degradation. Mechanisms at the elementary reaction level are established, which is of biological significance for understanding DNA damage involving C oxidation. Particularly for cytosine quadruplex i-motif, the revealed $C^{\bullet+}$ hydration pathway and the ensuing $C(5OH)^{\bullet}$ and $C(6OH)^{\bullet}$ formation point to deleterious consequences for altering the i-motif structure and stability, and the structure-dependent biological functions. We hope this work could arouse future research interests addressing cytosine oxidation in i-motif, which should be a topic with growing importance given the recent discovery of i-motif structure in human cells.

ASSOCIATED CONTENT

Supporting Information

The Supporting Information is available free of charge on the ACS Publications website at DOI: 10.1021/jacs.8b10743.

Calculated spectra, CD spectra, and additional transient absorption data (PDF)

AUTHOR INFORMATION

Corresponding Author

*hongmei@bnu.edu.cn

ORCID

Hongmei Su: 0000-0001-7384-6523

DOI: 10.1021/jacs.8b10743
J. Am. Chem. Soc. 2019, 141, 1970−1979

Author Contributions

‖These authors contributed equally.

Notes

The authors declare no competing financial interest.

■ ACKNOWLEDGMENTS

This work was financially supported by the National Natural Science Foundation of China (Grant Nos. 21425313, 21727803, 21333012, and 21773257).

■ REFERENCES

(1) Cadet, J.; Douki, T.; Ravanat, J.-L. Oxidatively generated base damage to cellular DNA. *Free Radical Biol. Med.* **2010**, *49*, 9.
(2) Lonkar, P.; Dedon, P. C. Reactive species and DNA damage in chronic inflammation: reconciling chemical mechanisms and biological fates. *Int. J. Cancer* **2011**, *128*, 1999.
(3) Zhang, Y.; Liu, L.; Guo, S.; Song, J.; Zhu, C.; Yue, Z.; Wei, W.; Yi, C. Deciphering TAL effectors for 5-methylcytosine and 5-hydroxymethylcytosine recognition. *Nat. Commun.* **2017**, *8*, 901.
(4) Gomez-Mendoza, M.; Banyasz, A.; Douki, T.; Markovitsi, D.; Ravanat, J.-L. Direct Oxidative Damage of Naked DNA Generated upon Absorption of UV Radiation by Nucleobases. *J. Phys. Chem. Lett.* **2016**, *7*, 3945.
(5) Choi, J.; Park, J.; Tanaka, A.; Park, M. J.; Jang, Y. J.; Fujitsuka, M.; Kim, S. K.; Majima, T. Hole Trapping of G-Quartets in a G-Quadruplex. *Angew. Chem., Int. Ed.* **2013**, *52*, 1134.
(6) Georgakilas, A. G.; O'Neill, P.; Stewart, R. D. Induction and Repair of Clustered DNA Lesions: What Do We Know So Far? *Radiat. Res.* **2013**, *180*, 100.
(7) Cadet, J.; Wagner, J. R.; Shafirovich, V.; Geacintov, N. E. One-electron oxidation reactions of purine and pyrimidine bases in cellular DNA. *Int. J. Radiat. Biol.* **2014**, *90*, 423.
(8) Yang, K.; Greenberg, M. M. Enhanced Cleavage at Abasic Sites within Clustered Lesions in Nucleosome Core Particles. *ChemBioChem* **2018**, *19*, 2061.
(9) Banyasz, A.; Martínez-Fernández, L.; Improta, R.; Ketola, T.-M.; Balty, C.; Markovitsi, D. Radicals generated in alternating guanine–cytosine duplexes by direct absorption of low-energy UV radiation. *Phys. Chem. Chem. Phys.* **2018**, *20*, 21381.
(10) Zheng, L.; Greenberg, M. M. DNA Damage Emanating From a Neutral Purine Radical Reveals the Sequence Dependent Convergence of the Direct and Indirect Effects of γ-Radiolysis. *J. Am. Chem. Soc.* **2017**, *139*, 17751.
(11) Zheng, L.; Greenberg, M. M. Traceless Tandem Lesion Formation in DNA from a Nitrogen-Centered Purine Radical. *J. Am. Chem. Soc.* **2018**, *140*, 6400.
(12) Greenberg, M. M. Pyrimidine nucleobase radical reactivity in DNA and RNA. *Radiat. Phys. Chem.* **2016**, *128*, 82.
(13) Kobayashi, K.; Tagawa, S. Direct observation of guanine radical cation deprotonation in duplex DNA using pulse radiolysis. *J. Am. Chem. Soc.* **2003**, *125*, 10213.
(14) Wu, L.; Liu, K.; Jie, J.; Song, D.; Su, H. Direct Observation of Guanine Radical Cation Deprotonation in G-Quadruplex DNA. *J. Am. Chem. Soc.* **2015**, *137*, 259.
(15) Kobayashi, K.; Yamagami, R.; Tagawa, S. Effect of base sequence and deprotonation of guanine cation radical in DNA. *J. Phys. Chem. B* **2008**, *112*, 10752.
(16) Kumar, A.; Sevilla, M. D. Proton-Coupled Electron Transfer in DNA on Formation of Radiation-Produced Ion Radicals. *Chem. Rev.* **2010**, *110*, 7002.
(17) Banyasz, A.; Ketola, T.-M.; Muñoz-Losa, A.; Rishi, S.; Adhikary, A.; Sevilla, M. D.; Martinez-Fernandez, L.; Improta, R.; Markovitsi, D. UV-Induced Adenine Radicals Induced in DNA A-Tracts: Spectral and Dynamical Characterization. *J. Phys. Chem. Lett.* **2016**, *7*, 3949.
(18) Sun, H.; Taverna Porro, M. L.; Greenberg, M. M. Independent Generation and Reactivity of Thymidine Radical Cations. *J. Org. Chem.* **2017**, *82*, 11072.
(19) Banyasz, A.; Martínez-Fernández, L.; Balty, C.; Perron, M.; Douki, T.; Improta, R.; Markovitsi, D. Absorption of Low-Energy UV Radiation by Human Telomere G-Quadruplexes Generates Long-Lived Guanine Radical Cations. *J. Am. Chem. Soc.* **2017**, *139*, 10561.
(20) Jie, J.; Liu, K.; Wu, L.; Zhao, H.; Song, D.; Su, H. Capturing the radical ion-pair intermediate in DNA guanine oxidation. *Sci. Adv.* **2017**, *3*, e1700171
(21) Sun, H.; Zheng, L.; Greenberg, M. M. Independent Generation of Reactive Intermediates Leads to an Alternative Mechanism for Strand Damage Induced by Hole Transfer in Poly(dA–T) Sequences. *J. Am. Chem. Soc.* **2018**, *140*, 11308.
(22) Banyasz, A.; Ketola, T.; Martínez-Fernández, L.; Improta, R.; Markovitsi, D. Adenine radicals generated in alternating AT duplexes by direct absorption of low-energy UV radiation. *Faraday Discuss.* **2018**, *207*, 181.
(23) Rokhlenko, Y.; Geacintov, N. E.; Shafirovich, V. Lifetimes and Reaction Pathways of Guanine Radical Cations and Neutral Guanine Radicals in an Oligonucleotide in Aqueous Solutions. *J. Am. Chem. Soc.* **2012**, *134*, 4955.
(24) Rokhlenko, Y.; Cadet, J.; Geacintov, N. E.; Shafirovich, V. Mechanistic Aspects of Hydration of Guanine Radical Cations in DNA. *J. Am. Chem. Soc.* **2014**, *136*, 5956.
(25) Cadet, J.; Davies, K. J. A.; Medeiros, M. H. G.; Di Mascio, P.; Wagner, J. R. Formation and repair of oxidatively generated damage in cellular DNA. *Free Radical Biol. Med.* **2017**, *107*, 13.
(26) Samson-Thibault, F.; Madugundu, G. S.; Gao, S.; Cadet, J.; Wagner, J. R. Profiling Cytosine Oxidation in DNA by LC-MS/MS. *Chem. Res. Toxicol.* **2012**, *25*, 1902.
(27) Kreutzer, D. A.; Essigmann, J. M. Oxidized, deaminated cytosines are a source of C → T transitions in vivo. *Proc. Natl. Acad. Sci. U. S. A.* **1998**, *95*, 3578.
(28) Wagner, J. R.; Hu, C. C.; Ames, B. N. Endogenous oxidative damage of deoxycytidine in DNA. *Proc. Natl. Acad. Sci. U. S. A.* **1992**, *89*, 3380.
(29) Madugundu, G. S.; Wagner, J. R.; Cadet, J.; Kropachev, K.; Yun, B. H.; Geacintov, N. E.; Shafirovich, V. Generation of Guanine–Thymine Cross-Links in Human Cells by One-Electron Oxidation Mechanisms. *Chem. Res. Toxicol.* **2013**, *26*, 1031.
(30) Wagner, J. R.; Cadet, J. Oxidation Reactions of Cytosine DNA Components by Hydroxyl Radical and One-Electron Oxidants in Aerated Aqueous Solutions. *Acc. Chem. Res.* **2010**, *43*, 564.
(31) Bose, A.; Basu, S. Medium-dependent interactions of quinones with cytosine and cytidine: A laser flash photolysis study with magnetic field effect. *Biophys. Chem.* **2009**, *140*, 62.
(32) Anderson, R. F.; Shinde, S. S.; Maroz, A. Cytosine-Gated Hole Creation and Transfer in DNA in Aqueous Solution. *J. Am. Chem. Soc.* **2006**, *128*, 15966.
(33) Aravindakumar, C. T.; Schuchmann, M. N.; Rao, B. S. M.; von Sonntag, J.; von Sonntag, C. The reactions of cytidine and 2′-deoxycytidine with $SO4^{\bullet-}$- revisited. Pulse radiolysis and product studies. *Org. Biomol. Chem.* **2003**, *1*, 401.
(34) Geimer, J.; Hildenbrand, K.; Naumov, S.; Beckert, D. Radicals formed by electron transfer from cytosine and 1-methylcytosine to the triplet state of anthraquinone-2,6-disulfonic acid. A Fourier-transform EPR study. *Phys. Chem. Chem. Phys.* **2000**, *2*, 4199.
(35) Naumov, S.; Hildenbrand, K.; von Sonntag, C. Tautomers of the N-centered radical generated by reaction of $SO4^{\bullet-}$- with N1-substituted cytosines in aqueous solution. Calculation of isotropic hyperfine coupling constants by a density functional method. *Journal of the Chemical Society, Perkin Transactions 2* **2001**, 1648.
(36) Adhikary, A.; Kumar, A.; Bishop, C. T.; Wiegand, T. J.; Hindi, R. M.; Adhikary, A.; Sevilla, M. D. π-Radical to σ-Radical Tautomerization in One-Electron-Oxidized 1-Methylcytosine and Its Analogs. *J. Phys. Chem. B* **2015**, *119*, 11496.
(37) Gehring, K.; Leroy, J.-L.; Gueron, M. A tetrameric DNA structure with protonated cytosine-cytosine base pairs. *Nature* **1993**, *363*, 561.
(38) Keane, P. M.; Wojdyla, M.; Doorley, G. W.; Kelly, J. M.; Parker, A. W.; Clark, I. P.; Greetham, G. M.; Towrie, M.; Magno, L. M.;

DOI: 10.1021/jacs.8b10743
J. Am. Chem. Soc. 2019, 141, 1970–1979

Quinn, S. J. Long-lived excited states in i-motif DNA studied by picosecond time-resolved IR spectroscopy. *Chem. Commun.* **2014**, *50*, 2990.
(39) Brooks, T. A.; Kendrick, S.; Hurley, L. Making sense of G-quadruplex and i-motif functions in oncogene promoters. *FEBS J.* **2010**, *277*, 3459.
(40) Abou Assi, H.; Garavís, M.; González, C.; Damha, M. J. i-Motif DNA: structural features and significance to cell biology. *Nucleic Acids Res.* **2018**, *46*, 8038.
(41) Zeraati, M.; Langley, D. B.; Schofield, P.; Moye, A. L.; Rouet, R.; Hughes, W. E.; Bryan, T. M.; Dinger, M. E.; Christ, D. I-motif DNA structures are formed in the nuclei of human cells. *Nat. Chem.* **2018**, *10*, 631.
(42) Kumar, A.; Sevilla, M. D. Cytosine Iminyl Radical (cytN•) Formation via Electron-Induced Debromination of 5-Bromocytosine: A DFT and Gaussian 4 Study. *J. Phys. Chem. A* **2017**, *121*, 4825.
(43) Wagner, J. R.; Decarroz, C.; Berger, M.; Cadet, J. Hydroxyl-Radical-Induced Decomposition of 2′-Deoxycytidine in Aerated Aqueous Solutions. *J. Am. Chem. Soc.* **1999**, *121*, 4101.
(44) Reilly, S. M.; Morgan, R. K.; Brooks, T. A.; Wadkins, R. M. Effect of Interior Loop Length on the Thermal Stability and pKa of i-Motif DNA. *Biochemistry* **2015**, *54*, 1364.
(45) Day, H. A.; Huguin, C.; Waller, Z. A. E. Silver cations fold i-motif at neutral pH. *Chem. Commun.* **2013**, *49*, 7696.
(46) Berdakin, M.; Steinmetz, V.; Maitre, P.; Pino, G. A. Gas Phase Structure of Metal Mediated $(Cytosine)_2Ag^+$ Mimics the Hemi-protonated $(Cytosine)_2H^+$ Dimer in i-Motif Folding. *J. Phys. Chem. A* **2014**, *118*, 3804.
(47) Giese, B.; Amaudrut, J.; Köhler, A.-K.; Spormann, M.; Wessely, S. Direct observation of hole transfer through DNA by hopping between adenine bases and by tunnelling. *Nature* **2001**, *412*, 318.
(48) Kawai, K.; Majima, T. Hole Transfer Kinetics of DNA. *Acc. Chem. Res.* **2013**, *46*, 2616.
(49) Joy, A.; Ghosh, A. K.; Schuster, G. B. One-Electron Oxidation of DNA Oligomers That Lack Guanine: Reaction and Strand Cleavage at Remote Thymines by Long-Distance Radical Cation Hopping. *J. Am. Chem. Soc.* **2006**, *128*, 5346.
(50) Dvořáková, Z.; Renčiuk, D.; Kejnovská, I.; Školáková, P.; Bednářová, K.; Sagi, J.; Vorlíčková, M. i-Motif of cytosine-rich human telomere DNA fragments containing natural base lesions. *Nucleic Acids Res.* **2018**, *46*, 1624.

DOI: 10.1021/jacs.8b10743
J. Am. Chem. Soc. 2019, 141, 1970−1979